

Rupture Directivity of the 3 November 2002 Denali Fault Earthquake Determined from Surface Waves

by Aaron A. Velasco, Charles J. Ammon, Jamie Farrell, and Kris Pankow

Abstract The M_w 7.9 earthquake that struck central Alaska on 3 November 2002 was preceded 11 days earlier by an M_w 6.7 strike-slip foreshock on 23 October 2002. Both events were predominantly strike-slip and ruptured structures associated with the Denali fault system. Previous studies have shown that the mainshock began with failure on a relatively small northeast-striking reverse fault, before breaking out for 300 km of right-lateral strike-slip rupture. Aftershock patterns suggest that the foreshock ruptured a region west of the mainshock, which began near the eastern extent of the foreshock sequence and proceeded east-southeast. To constrain and to quantify source duration and directivity effects, we examine surface-wave displacement seismograms and use an empirical Green's function (EGF) to isolate and explore mainshock rupture kinematics. Our particular interest lies in large-amplitude focussing caused by directivity. We observe Love and Rayleigh wave amplification of two orders of magnitude in the period range from 10 to 33 sec. These remarkable directivity-enhanced surface waves triggered small earthquakes more than 3000 km from the mainshock rupture.

Introduction

The 3 November 2002 Denali fault earthquake (M_w 7.9 [Harvard Centroid Moment Tensor (CMT) catalog], M_S 8.5 [U.S. Geological Survey (USGS)]) occurred in a remote region of central Alaska and was the largest North American strike-slip earthquake since the 1906 San Francisco event (National Earthquake Information Center [NEIC] historic and Preliminary Determination Earthquake catalogs). The Denali fault earthquake ruptured a 300-km-long segment of the Denali fault system and accommodated a trench parallel component of the Pacific-North American plate motion (Eberhart-Philips *et al.*, 2003). Studies of the source process suggest a complex rupture (Ozacar *et al.*, 2003; Hreinsdóttir *et al.*, 2003). The event began with reverse slip and then evolved into a unilateral strike-slip rupture that eventually accumulated slip on three faults (Eberhart-Philips *et al.*, 2003; Ozacar *et al.*, 2003). The earthquake's effects were widespread and included numerous induced landslides, a broad area of liquefaction (Harp *et al.*, 2003), and triggered seismicity in several areas of the conterminous United States (e.g., Pankow *et al.*, 2004; Prejean *et al.*, 2004; Husen and Wiemer, 2004; Husker and Brodsky, 2004). Remote earthquake triggering appears to have been restricted to areas south of the epicenter, suggesting that the cause is related to the rupture style and directivity (Gomberg *et al.*, 2004; Pankow *et al.*, 2004; Prejean *et al.*, 2004; and Husen and Wiemer, 2004).

Studies of large strike-slip earthquakes show that at least

some of these intraplate events trigger earthquakes at remote distances. A well-documented example is the 1992 Landers earthquake, which triggered a series of seismic events that corresponded in time to the passage of the surface waves (e.g., Hill *et al.*, 1993; Anderson *et al.*, 1994). Seismicity triggering for this event occurred in the direction of strong directivity (e.g., Velasco *et al.*, 1994). In this article, we document our analysis of Rayleigh and Love waves from the Denali fault earthquake to quantify the strong directivity effects. The strong directivity effects for this event are compatible with a long unilateral rupture propagating with a typical rupture velocity (about 3 km/sec). The combined Love wave-radiation pattern and directivity effects produced substantial Love wave-associated deformation that resulted in high peak dynamic stresses (PDS) along azimuths aligned near the rupture direction.

Surface-Wave Observations

An unfortunate consequence of the substantial Love-wave amplitudes is that several seismic recording systems were driven off scale. (This is also a function of the instrument gain setting.) Many of the clipped signals were recorded at stations that lie near a great circle path aligned with the direction of rupture; some were located as far from the source as ~ 3400 km. Among the stations with signal clipping, all east components were off scale (Love waves),

but only select north and vertical components clipped (Rayleigh waves). For our analyses, we used only on-scale observations from the western United States (broadband seismometer data from the U.S. National Seismic Network [USNSN]) along with a global distribution of stations obtained from the Global Seismic Network Stations (GSN).

Rupture directivity is essentially a Doppler effect, where a unilateral rupture that propagates along a fault will show higher amplitudes and shorter durations for stations located at an azimuth of the rupture propagation. To investigate this effect for this earthquake, we begin with a simple analysis of the Rayleigh and Love wave-amplitude variations caused by the rupture propagation. We measured the peak-to-peak displacement amplitude of the surface waves (group-velocity windows of 5.3 and 2.5 km/sec for the Love waves and 4.5 and 2.0 km/sec for the Rayleigh waves) in the period bands of 10–20, 20–33, 33–50, 50–100, 100–200, and 200–300 sec. We corrected the amplitudes for a radiation pattern, using approximately a $\sin 4\theta$ function, which is appropriate for the Harvard moment tensor solution (Table 1). We also corrected for geometrical spreading to an effective distance of 30° (each signal is scaled by $\sqrt{\sin \Delta / \sin 30^\circ}$), where Δ is the distance from the source to the station. We then corrected for attenuation ($\exp(\omega_0 x / 2cQ)$), where ω_0 is the center period of our passband, x is the great circle arc distance, c is the average group velocity (4.35 km/sec and 3.65 km/sec for Love and Rayleigh waves, respectively), and Q is the quality factor. For this period range, we chose Q to be constant at periods of 150 and 130 sec for Love and Rayleigh waves, respectively; this is an approximate average from the Preliminary Reference Earth Model (PREM) (Dziewonski and Steim, 1982). To first order, the remaining amplitude variation reflects only source depth and directivity effects. For our simple analysis we ignore depth dependence, which will affect the amplitudes as a function of period; we are primarily interested in looking at the directivity as a function of azimuth for particular period bands.

Figure 1 shows the normalized amplitude versus azimuth from the source for the six period bands. The long horizontal lines in each panel represent the approximate amplitude baselines, and the shorter lines show the approximate peak amplitude levels between 90° and 125° azimuth. The directivity effect produces amplifications up to two orders of magnitude from 10 to 33 sec, and the effect falls off as the periods increase. The amplitudes were enhanced from

90° to 120° azimuth for both the Love and Rayleigh waves. The wide azimuthal range of amplification is consistent with the curvature of the fault plane and much wider than previously noted (Gomberg *et al.*, 2004). The observation is consistent with groundwater disturbances as far east as Pennsylvania, which were widely reported in the media. Obvious seismicity triggering seems to have been restricted to the region of the western Cordillera (Gomberg *et al.*, 2004). The dramatic amplification produced ground motions on the order of 5 cm at distances of several thousand kilometers. Pankow *et al.* (2004) show that the microseismic activity in Utah began with the arrival of these large-amplitude Love waves. Prejean *et al.* (2004) also document the onset of the triggering with the passage of the Love and Rayleigh waves having a dominant period of 15 to 40 sec.

We calculated PDS values associated with the surface waves using the method of Hill *et al.* (1993). In this method, one assumes that the Love waves propagate as a planar shear wave. For longer period waves ($T > 20$ sec) this is a reasonable approximation (Hill *et al.*, 1993). The amplitude decrease with depth is small in the crust. The relationship between PDS and peak velocity is given by:

$$\text{PDS} = \bar{v} \frac{\mu}{\beta} \quad (1)$$

where \bar{v} is the peak velocity vector (sum of the three-component velocity records), μ is the rigidity, and β is the shear-wave velocity. Choosing μ as 3.3×10^{11} dynes cm^2 and β as 3.5×10^5 cm/sec, the ratio of $\mu/\beta \approx 0.1$ (MPa/cm/sec) and PDS is approximately equal to the peak vector velocity.

Thus, the peak velocity vector magnitude provides a reasonable estimation of the peak dynamic surface stress associated with the surface waves. Even the clipped signals can be used to provide information on the minimum dynamic stress. A contour map of the resulting PDS across the western conterminous United States is given in Figure 2. Also shown are the stations whose signals were clipped. Seismograms recorded by stations as far away as ~ 3400 km were clipped during the passage of the Love waves. For these records, all were clipped on the east–west component, whereas some were also clipped on the north–south and vertical components. These clipping signals were recorded by stations

Table 1
USGS and Harvard Source Parameters

Earthquake	NEIC				Harvard CMT						
	Lat.	Lon.	Depth	Date/Time (mm/dd/yy)	M_S	M_o	M_w	str	dip	rk	
Denali fault	63.52	-147.53	5.0	11/03/02 22:12:41	8.5	7.48×10^{27}	7.9	29	82	19	
Nenana Mt.	63.62	-148.04	10.0	10/20/02 11:27:18	6.7	1.09×10^{26}	6.6	352	89	1	

Lat., latitude; Lon., longitude; str, strike (degrees); dip (degrees); rk, rake (degrees); M_o , moment in dyne cm.

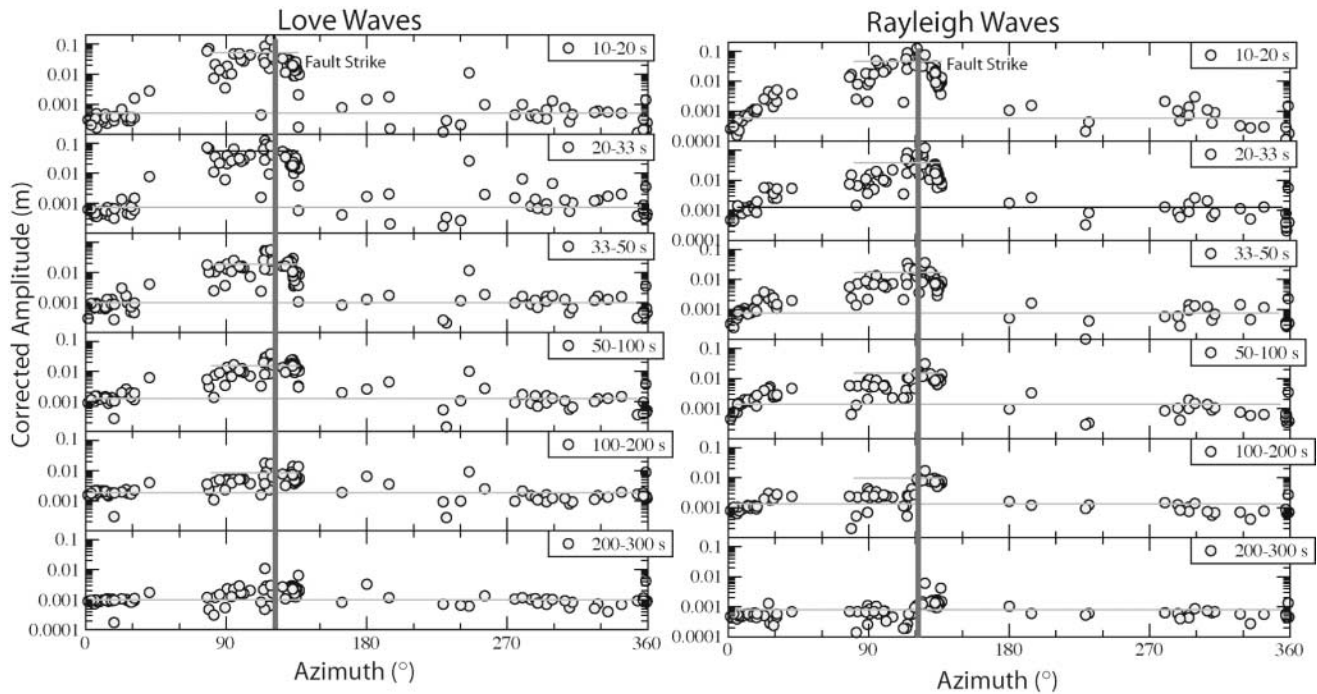


Figure 1. Normalized peak-to-peak amplitudes of Love (a) and Rayleigh (b) waves as a function of azimuth from the mainshock. The amplitudes are corrected for mechanism and attenuation effects and have been normalized to 30° distance to correct for geometrical spreading. Note the two orders of magnitude amplitude difference caused by the rupture directivity.

which lie on or near the projected path of directivity, as derived from the fault plane determined by the Harvard centroid moment tensor (Table 1). First, we see an increase in the PDS values along projected mainshock strike. A similar pattern was constructed by using seismograms and continuous Global Positioning System (GPS) observations (Gomberg *et al.*, 2004). The PDS values range from 0.2 to 0.3 MPa in Wyoming and Utah to values as low as 0.015 to 0.05 MPa at a similar distance in California. These values show variability on the order of 10 to 20 in this azimuth range. The PDS value difference is large enough to trigger microseismic activity in Wyoming and Utah (Pankow *et al.*, 2004), and in some regions in California (Prejean *et al.*, 2004).

Empirical Green's Function Analysis

To equalize propagation effects and to extract information on the rupture kinematics, we applied an empirical Green's function (EGF) analysis (e.g., Hartzell, 1978; Mueller 1985; Hough *et al.*, 1991; Ammon *et al.*, 1993; Velasco *et al.*, 1994, 1995, 1996, 2000) to regional and teleseismic body and surface waves recorded by the GSN and USNSN networks. The EGF method exploits signals from a smaller nearby earthquake having a similar focal mechanism and centroid depth to account for poorly known excitation and propagation effects. We refer to the resulting functions as

relative source-time functions (RSTFs) because the mainshock rupture information is recovered only in a sense relative to the smaller event. We used a frequency domain water-level method (Helmberger and Wiggins, 1971; Clayton and Wiggins, 1976) with a water-level value of 0.001 to deconvolve the EGF signals from the mainshock signals.

We examined two candidate EGFs for our analysis (Fig. 3); neither EGF event is ideal. The first event occurred on 5 July 2002 (M_w 5.8) near the mainshock epicenter. Given the size of this event, the signal-to-noise ratio for most global stations is poor, limiting its application to signals from relatively nearby stations. The second event is the M_w 6.7 Nenana Mountain earthquake that occurred on 23 October 2002 about 30 km to the west of the mainshock epicenter (Table 1). The size discrepancy between the mainshock and the Nenana Mountain earthquake EGF introduces several complications to RSTF interpretation. The Denali fault earthquake ruptured a long, curved fault and thus incorporated substantial fault strike variation relative to any smaller, constant-strike, planar EGF. It initiated with a reverse-faulting subevent, followed by the dominant moment release, which was strike-slip (Ozacar *et al.*, 2003). The 300-km length of the fault means that both EGFs are closer to one end of the rupture than the fault centroid. The large magnitude of the Nenana Mountain earthquake means that its rupture characteristics must be removed by working with the long-period portion of the signal. We performed a simple

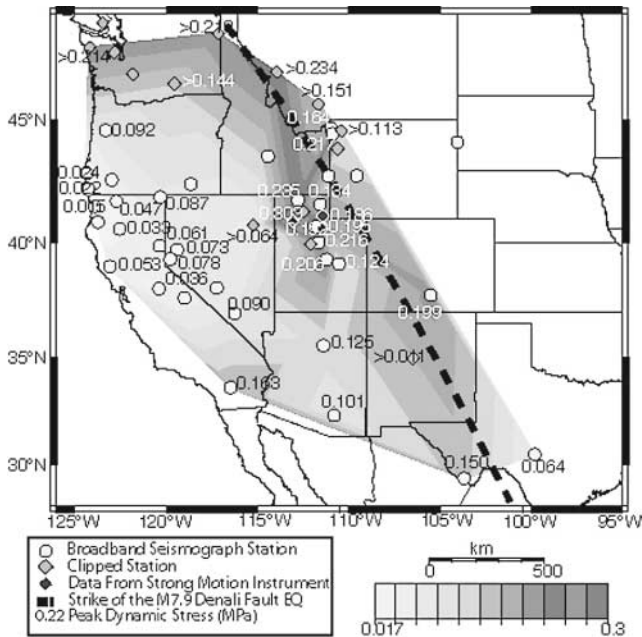


Figure 2. Peak dynamic stress (PDS) values calculated for western United States seismic stations after the passage of the M_w 7.9 Denali fault earthquake Love waves. Because of these Love waves, seismic records were clipped for stations as far away as ~ 3400 km from the source. Stations are color contoured to show PDS values in MPa. Diamonds are broadband seismic stations whose signals were clipped, and circles represent those that were not clipped. For records that were clipped the recorded PDS values are minima (see text). Raw east-component waveforms are shown for selected clipped records. Units are 10^6 counts. Duration is shown for each trace. The stations exhibiting clipping follow the projected path of directivity (dashed line) based on the fault plane determined by the Harvard CMT.

sensitivity analysis to explore the limitations of this EGF and found that the sacrifice of information from periods below 30 sec allows us to image the rupture in the intermediate-period band from 30 to 150 sec, which is often difficult to resolve in body-wave and strong-motion studies. We still have amplitude complications due to changes in mechanism, so we focus on the simplest features in the RSTFs.

We applied a directivity analysis that uses pulse-width variation of the source-time functions to determine the azimuth of rupture and the distance between time features (e.g., Schwartz and Ruff, 1985; Ammon *et al.*, 1993; Velasco *et al.*, 1994). For our time features, we chose the onset and end of the RSTFs. We obtained a rupture azimuth of $122 \pm 25^\circ$, which corresponds to a linear correlation coefficient of 0.95. The direction is remarkably consistent with the strike of the Harvard CMT solution considering the complications in the EGF. The total rupture duration is formally 80 ± 2 sec, and the rupture length is estimated to be 216 ± 7 km. The formal uncertainties are certainly overstated, because we have in-

cluded the 30-sec low-pass filter in the RSTFs and our results may be on the order of 10 sec too long. Maps of surface rupture provide a very detailed picture of the rupture for this event, so the average value recovered in the RSTF analysis has limited impact. However, the result shows that the basic information available from the RSTFs provides important, propagation-corrected constraints to the magnitude of directivity associated with this event.

Directivity can be seen directly in the averaged RSTFs (Fig. 4). Assuming a rupture direction of 121° (the strike of the Harvard CMT mechanism), we stacked the RSTFs as a function of the directivity parameter, $\Gamma = \cos \theta/c$, where θ is the azimuth relative to the rupture direction and c is the wave-phase velocity. To minimize amplitude distortions, we normalized each RSTF to unit amplitude at the longest periods before binning and averaging. The stacks are aligned with what we estimate to be the beginning of the strike-slip component of the mainshock. We venture little quantitative interpretation because of the EGF limitations described previously, but we note that the RSTFs show at least 60 sec of directivity, which is due to the unilateral rupture propagating near the group velocity of the surface waves.

Although the length and curvature of the mainshock and possible directivity in the EGF complicate azimuthal patterns in the RSTFs, the effects are minimized for station KONO (Kongsberg, Norway, at a distance of 55.7°), which is located roughly perpendicular to the rupture. Directivity effects in both the mainshock and EGF are minimal for this station, and neither mechanism is nearly nodal. The distance from KONO to the EGF is also roughly the same for the entire length of the mainshock fault. Because of this fortuitous geometry, we used the KONO RSTF to estimate the slip along strike of the Denali fault earthquake. To estimate slip, we use the formulation of Velasco *et al.* (1994) given by:

$$S(v_r t) = \frac{f_{\perp}(t)}{v_r \mu W} \quad (2)$$

where $f_{\perp}(t)$ is the source-time function perpendicular to the fault, v_r is the rupture velocity, μ is the shear modulus, and W is the fault width. In this case, we use the KONO RSTF as our source-time function ($f_{\perp}(t)$), μ as 3.3×10^{11} dynes cm^2 , and v_r as 3.2 km/sec.

Figure 5 shows the estimated slip. To obtain $f_{\perp}(t)$, we fix the area under the RSTF to be consistent with the Harvard CMT moment (Table 1). The shape of the slip is generally compatible with surface observations. However, the RSTF slip amplitude is substantially higher unless we assume a rather thick seismogenic zone of 25 km. The curve corresponding to a fault width of 20 km is reasonably consistent with the larger magnitudes of slip observed along the surface. The similarity in the pattern of slip adds to our confidence in the RSTF results, but the results suggest that the surface slip is less than that which occurred at depth.

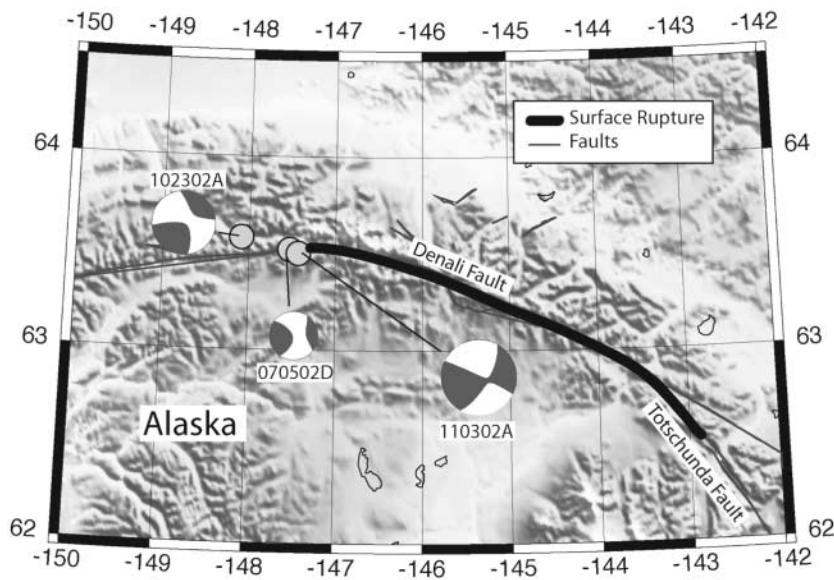


Figure 3. Base map showing the faults in the region, the mainshock epicenter, and two possible EGFs. The large black line represents the surface rupture (from Eberhart-Phillips *et al.*, 2003), whereas the thinner lines represent faults. Focal mechanisms are from the Harvard CMT catalog (Table 1).

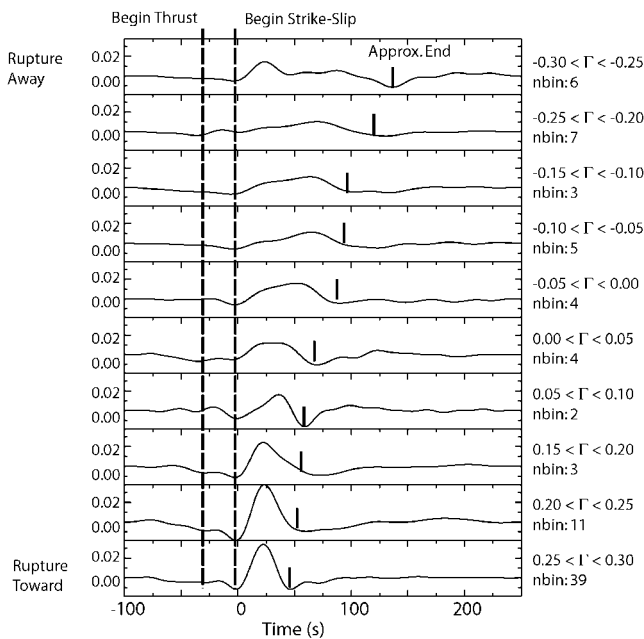


Figure 4. Stacked RSTFs plotted as a function of the directivity parameter, Γ , assuming a strike of 121° . The number of observations in each bin is noted (NBIN). The dashed lines represent the onset of the thrust event and the onset of the strike-slip component of rupture. The short line at the end of the RSTFs represents the approximate end of the rupture. Note the strong unilateral component of rupture, with durations from 170 to 45 sec.

Discussion

For the 1992 Landers earthquake, Hill *et al.* (1993) and Anderson *et al.* (1994) documented a significant increase in seismicity throughout the western Great Basin. Anderson *et al.* (1994) proposed that this increase was associated with

dynamic stresses caused by the passage of large-amplitude waves crossing the region. Much of the triggered seismicity was north of the epicenter, in the direction of directivity (Velasco *et al.*, 1994). The Denali fault earthquake repeats this pattern. In the first 24 hr after the passage of Love waves more than 250 earthquakes occurred in the Yellowstone National Park region (Husen and Wiemer, 2004). In Utah, the average seismicity rate across the state increased by a factor of 10 in the first 24 hr and remained at an elevated level for 25 days in most areas (Pankow *et al.*, 2004). Rupture-amplified surface waves play a key role in remote dynamic triggering of earthquakes (e.g., Gomberg *et al.*, 2001).

Our work on the Denali fault earthquake shows that the directivity is large for periods between 20 and 50 sec and is largest in the range of 15 to 30 sec. Prejean *et al.* (2004) document the onset of triggering from the Denali fault earthquake at several volcanic and geothermal centers in Washington and California coincident with the passage of Love and Rayleigh waves having a dominant period of 15 to 40 sec. Thus, triggering caused by surface waves appears to be frequency dependent and, in this case, arises because of significant amplification of the surface waves at 10–50 sec periods as a result of rupture directivity. To investigate the importance of duration on the triggering phenomena, we note that the eastern Basin and Range experienced significantly different duration of high dynamic stresses for the Landers and Denali fault earthquakes. The duration of strong shaking in period range from 15 to 50 sec (the range experiencing the strongest directivity [Fig. 1]) in the eastern Basin and Range was on the order of 3 to 4 min for the Denali fault earthquake, whereas shaking caused by the Landers earthquake in the same region probably lasted only one third as long, because the same group velocity range would have extended for a duration of only one third of that of the Denali fault earthquake. The fact that both events triggered seis-

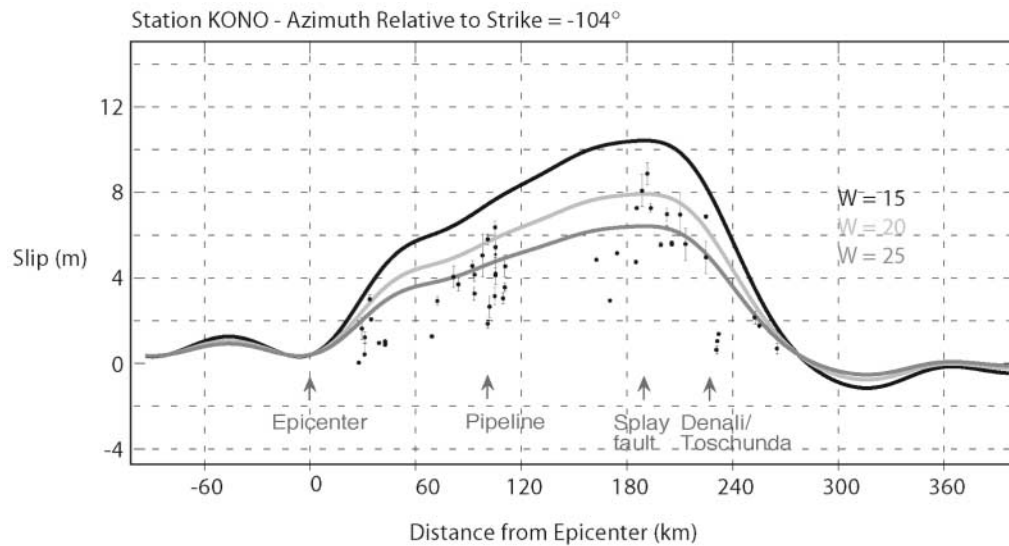


Figure 5. Slip estimates derived from one RSTF that is perpendicular to the fault, assuming different fault widths. Surface observations (dots) are also plotted. Using 15 km for a fault width results in a maximum slip of more than 10 m.

micity in the Yellowstone region suggests that durations on the order of 1 min are capable of disturbing the equilibrium. It remains to be seen whether any differences in the longevity or intensity of the Denali fault earthquake-induced activity arise from the longer shaking.

Our EGF analysis also suggests the existence of higher slip than inferred from the surface observations and/or a deeper rupture than would be inferred from the aftershocks, which occurred principally at depths less than 7 km (Ratchkovski *et al.*, 2003). This conclusion is more a consequence of the Harvard CMT seismic moment than of the EGF analysis. The EGF provides the slip shape, which agrees well with that reflected in the surface slip. Equalizing the area of the RSTF to the Harvard moment and then transforming to slip leads to our conclusions regarding the subsurface-slip extent. The existence of a substantial component of deeper, smooth slip may help to explain the remarkable directivity associated with this event.

Conclusions

We quantify strong Rayleigh and Love directivity from the Denali fault earthquake caused by a long, unilateral rupture. Directivity accounts for up to two orders of magnitude increase in amplitude of the Rayleigh and Love waves between the periods of 10–33 sec. Our analysis using the GSN suggests that large displacements were radiated across a broad azimuthal corridor extending into eastern North America. Given the coincidence of remotely triggered regions in the western United States with the path of directivity, we conclude that the combined Love wave radiation, nature of the source-time function, and the directivity effects cause large surface-wave amplitudes that were responsible for much of the earthquake triggering. Accepting the Har-

vard estimate of moment, an EGF analysis suggests that either the surface-slip underestimates the slip at depth or the rupture extends to at least twice the depth of the majority of aftershocks.

Acknowledgments

We thank Robert Smith for helpful discussions, Harley Benz for providing the western U.S. data, and the Data Management Center (DMC) of the Incorporated Research Institutions of Seismology for the Global Seismic Network (GSN) data. We also thank K. Shabestari and an anonymous reviewer for constructive comments.

References

- Anderson, J. G., J. N. Brune, J. N. Louie, Y. Zeng, M. Savage, G. Yu, Q. Chen, and D. dePolo (1994). Seismicity in the western Great Basin apparently triggered by the Landers, California earthquake, 28 June 1992, *Bull. Seism. Soc. Am.* **84**, 863–891.
- Ammon, C. J., A. A. Velasco, and T. Lay (1993). Rapid estimation of rupture directivity: Application to the 1992 Landers ($M_s = 7.4$) and Cape Mendocino ($M_s = 7.2$) California earthquakes, *Geophys. Res. Lett.* **20**, 97–100.
- Clayton, R. W., and R. A. Wiggins (1976). Source shape estimation and deconvolution of teleseismic body waves, *Geophys. J. R. Astr. Soc.* **47**, 151–177.
- Dziewonski, A. M., and J. M. Steim (1982). Dispersion and attenuation of mantle waves through waveform inversion, *R. Astr. Soc. Geophys. J.* **76**, 399–438.
- Eberhart-Phillips, D., P. J. Haeussler, J. T. Freymueller, A. D. Frankel, C. M. Rubin, P. Craw, N. A. Ratchkovski, G. Anderson, G. A. Carver, A. J. Crone, T. E. Dawson, H. Fletcher, R. Hansen, E. L. Harp, R. A. Harris, D. P. Hill, S. Hreinsdóttir, R. W. Jibson, L. M. Jones, R. E. Kayen, D. K. Keefer, C. F. Larsen, S. C. Moran, S. F. Personius, G. Plafker, B. L. Sherrod, K. Sieh, N. Sitar, and W. K. Wallace (2003). The 2002 Denali fault earthquake, Alaska: a large magnitude, slip-partitioned event, *Science* **300**, 1113–1118.
- Gomberg, J., P. Bodin, K. Larson, and H. Dragert (2004). Earthquake nu-

- creation by transient deformations caused by the $M = 7.9$ Denali, Alaska, earthquake, *Nature* **427**, 621–624.
- Gomberg, J. S., P. A. Reasenberg, P. Bodin, and R. A. Harris (2004). Earthquake triggering by seismic waves following the Landers and Hector Mine earthquakes, *Nature* **411**, 462–466.
- Harp, E. L., R. W. Jibson, R. E. Kayen, D. K. Keffer, B. L. Sherrod, G. A. Carver, B. D. Collins, R. E. S. Moss, and N. Sitar (2003). Landslides and liquefaction triggered by the $M 7.9$ Denali fault earthquake of 3 November 2002, *GSA Today* **13**, 4–10.
- Hartzell, S. (1978). Earthquake aftershocks as Green's functions, *Geophys. Res. Lett.* **5**, 1–5.
- Helmberger, D., and R. A. Wiggins (1971). Upper mantle structure of the mid-western United States, *J. Geophys. Res.* **76**, 3229–3245.
- Hill, D. P., P. A. Reasenberg, A. Michael, W. J. Arabaz, G. Beroza, D. Brumbaugh, J. N. Brune, R. Castro, S. Davis, D. dePolo, W. L. Ellsworth, J. Gomberg, S. Harmsen, L. House, S. M. Jackson, M. J. S. Johnston, L. Jones, R. Keller, S. Malone, L. Munguia, S. Nava, J. C. Pechmann, A. Sanford, R. W. Simpson, R. B. Smith, M. Stark, M. Stickney, A. Vidal, S. Walter, V. Wong, and J. Zollweg (1993). Seismicity remotely triggered by the magnitude 7.3 Landers, California earthquake, *Science* **260**, 1617–1623.
- Hough, S. E., L. Seeber, and A. Lerner-Lam (1991). Empirical Green's function analysis of Loma Prieta aftershocks, *Bull. Seism. Soc. Am.* **81**, 1737–1753.
- Hreinsdóttir, S., J. T. Freymueller, H. J. Fletcher, C. F. Larsen, and R. Burgmann (2003). Coseismic slip distribution of the 2002 $M_w 7.9$ Denali fault earthquake, Alaska, determined from GSP measurements, *Geophys. Res. Lett.* **30**, 3-1–3-4.
- Husen, S., and S. Wiemer (2004). Remotely triggered seismicity in the Yellowstone National Park region by the 2002 $M_w = 7.9$ Denali fault earthquake, Alaska, *Bull. Seism. Soc. Am.* **94**, no. 6B, S317–S331.
- Husker, A. L., and E. E. Brodsky (2004). Triggered seismicity in Idaho and Montana: a window into the geologic context for seismic triggering, *Bull. Seism. Soc. Am.* **94**, no. 6B, S310–S316.
- Mueller, C. S. (1985). Source pulse enhancement by deconvolution of an empirical Green's function, *Geophys. Res. Lett.* **12**, 33–36.
- Ozacar, A. A., S. L. Beck, and D. H. Christensen (2003). Source process of the 3 November 2002 Denali fault earthquake from teleseismic observations, *Geophys. Res. Lett.* **30**, no. 1638, 40-1–40-4.
- Pankow, K. L., W. J. Arabasz, J. C. Pechmann, and S. J. Naval (2004). Triggered seismicity in Utah from the 3 November 2002 Denali fault earthquake, *Bull. Seism. Soc. Am.* **94**, no. 6B, S332–S347.
- Prejean, S. G., D. P. Hill, E. E. Brodsky, S. E. Hough, M. J. S. Johnston, S. D. Malone, D. H. Oppenheimer, A. M. Pitt, and K. B. Richards-Dinger (2004). Remotely triggered seismicity on the United States west coast following the $M 7.9$ Denali fault earthquake, *Bull. Seism. Soc. Am.* **94**, no. 6B, S348–S359.
- Ratchkovski, N. A., R. A. Hansen, J. C. Stachnik, T. Cox, O. Fox, L. Rao, E. Clark, M. Lafevers, S. Estes, J. B. MacCormack, and T. Williams (2003). Aftershock sequence of the $M_w 7.9$ Denali fault, Alaska, earthquake of 3 November 2002 from regional seismic network data, *Seism. Res. Lett.* **74**, 743–752.
- Schwartz, S. Y., and L. J. Ruff (1985). The 1968 Tokachi-Oki and the 1969 Kurile Islands earthquakes: variability in the rupture process, *J. Geophys. Res.* **90**, 8613–8626.
- Velasco, A. A., C. J. Ammon, and S. L. Beck (2000). Broadband source modeling of the November 8, 1997 Tibet ($M_w = 7.5$) earthquake and its tectonic implications, *J. Geophys. Res.* **105**, 28,065–28,080.
- Velasco, A. A., C. J. Ammon, and T. Lay (1994). Empirical Green function deconvolutions of broadband surface waves: rupture directivity of the 1992 Landers, California ($M_w = 7.3$) earthquake, *Bull. Seism. Soc. Am.* **84**, 735–750.
- Velasco, A. A., C. J. Ammon, and T. Lay (1995). Source time function complexity of the great 1989 Macquarie Ridge earthquake, *J. Geophys. Res.* **100**, 3989–4009.
- Velasco, A. A., C. J. Ammon, T. Lay, and M. Hagarty (1996). Rupture process of the 1990 Luzon, Philippines earthquake, *J. Geophys. Res.* **101**, 22,419–22,434.
- University of Texas at El Paso
El Paso, Texas 79968
(A.A.V.)
- The Pennsylvania State University
University Park, Pennsylvania 16802
(C.J.A.)
- University of Utah
Salt Lake City, Utah 84112
(J.F., K.P.)

Manuscript received 16 March 2004.